SIViP (2014) 8:923–930
DOI 10.1007/s11760-012-0337-x

ORIGINAL PAPER

Performance analysis of wave atom transform in texture classification

J. Rajeesh · R. S. Moni · S. S. Kumar

Received: 11 February 2011 / Revised: 25 April 2012 / Accepted: 27 April 2012 / Published online: 15 May 2012

Abstract Texture classification is an important application in image processing and pattern recognition such as detection of defects on the materials and diseases from the medical images. This paper presents the performance of wave atom transform on texture classification. Wave atom transform is a new multi-resolution technique that not only captures the coherence of the pattern along the oscillations, but also the pattern across the oscillations. The classification is done using a wave atom–transformed features reduced by singular value decomposition and a support vector machine. Experimental results are presented to demonstrate the effectiveness of this approach on Brodatz database, Alzheimer's Disease Neuro Imaging database for Alzheimer's disease classification and liver computed tomography images for tumor classification. The experimental results demonstrate that the proposed approach gives a percent correct classification of 97.29 % on Brodatz database, classification accuracy of 94 % on Alzheimer's Disease Neuro Imaging database for Alzheimer's disease diagnosis and 93.3 % on liver computed tomography images for tumor classification.

Keywords Alzheimer's disease · Computed tomography images · Magnetic resonance imaging · Wave atom transform

J. Rajeesh (✉) · R. S. Moni
Department of ECE, Noorul Islam College of Engineering, Kumaracoil 629180, India
e-mail: rajeesh_j@rediffmail.com

R. S. Moni
e-mail: moni2006_r_s@yahoo.co.in

S. S. Kumar
Department of EIE, Noorul Islam College of Engineering, Kumaracoil 629180, India
e-mail: kumar_s_s@hotmail.com

1 Introduction

Texture analysis is an important issue with applications ranging from remote sensing and crop classification to object-based image coding and tissue recognition in medical images. The primary objective of different methods presented is the rotation and gray-scale invariant texture analysis. As a fundamental basis for all texture-related applications, texture analysis seeks to derive a general, efficient, and compact quantitative description of the textures so that various mathematical operations can be used to alter, compare, and transform them. Most available texture analysis algorithms involve extracting the features and deriving an image coding scheme for representing the selected features. These algorithms may differ in the choice of features and the way of their representation. For example, a statistical approach [1] describes a texture through image signal statistics that reflect the non-deterministic properties of spatial distribution of image signals, and Markov random field models [2] consider spatial interactions over relatively small neighborhoods. Structural approaches [3] are based on regular or semi-regular placements of textural primitives. In the case of observable or visual textures, it is usually quite difficult to extract the primitives and their placements. These approaches are suitable only for highly regular deterministic textures. To reduce these problems, signal processing methods such as spatial domain filtering, frequency domain filtering and spatial-frequency domain filtering were proposed by many researchers [4,5].

The weakness of spatial and frequency domain filtering is that the image is analyzed at one single scale. To overcome these limitations, multi-resolution techniques were used [6,7]. In multi-resolution-based methods, sub-band energy is the most commonly used feature for texture classification problems. Hidden Markov models [8], generalized Gaussian

density-based model [9], histogram-based model [10], and hybrid IMM/SVM-based model [11] are some of the wavelet domain models proposed for texture classification. They require large number of features and training samples even for a moderate database. To overcome these problems, a texture classification method based on wavelet transformation and singular value decomposition (SVD) is proposed [12]. Wavelet in two dimensions has limited ability in capturing directional information. In this paper, we propose an alternate method using wave atom transform [13], which is a multi-resolution technique, has the ability to adapt to arbitrary local directions of pattern, and to sparsely represent anisotropic patterns aligned with the axes.

The paper is organized as follows. Section 2 describes the theory of wave atom transform and a brief about SVD and support vector machine (SVM) used in this work. Section 3 deals with the experiments performed on synthetic images, magnetic resonance images (MRI) images, and computed tomography (CT) images with their results. Section 4 ends with the conclusion.

2 Theory

2.1 Wave atom

Demanet and Ying [13] introduced so-called wave atoms that can be seen as a variant of 2-D wavelet packets and obey the parabolic scaling of curvelets wavelength $\sim$ (diameter)^2. Oscillatory functions or oriented textures (e.g., fingerprint, seismic profile, engineering surfaces) have a significantly sparser expansion in wave atoms than in other fixed standard representations like Gabor filters, wavelets, and curvelets.

Wave atoms have the ability to adapt to arbitrary local directions of a pattern, that is, warping. In comparison with curvelets, wave atoms not only capture the coherence of the pattern along the oscillations, but also the pattern across the oscillations. In the following, we shortly summarize the wave atom transform as recently suggested in [13].

Consider a 1-D family of wave packets $\psi^j_{m,n}(x)$, $j \geq 0, m \geq 0, n \in N$, centered in frequency around $\pm\omega_{j,m} = \pm\pi 2^j m$ with $c_1 2^j \leq m \leq c_2 2^j$ (where $c_1 < c_2$ are positive constants) and centered in space around $x_{j,n} = 2^{-j}n$. For that purpose, let g be a real-valued C^∞bump function with compact support in $[-7\pi/6, 5\pi/6]$ such that for $|\omega| \leq \pi/3$

$$g\left(\frac{\pi}{2}-\omega\right)^2 + g\left(\frac{\pi}{2}+\omega\right) = 1 \tag{1}$$

$$g\left(-\frac{\pi}{2}-2\omega\right) = g\left(\frac{\pi}{2}+\omega\right) \tag{2}$$

Then the function $\hat{\psi}^0_m$ is determined by the formula

$$\hat{\psi}^0_m(\varpi) := \mathrm{e}^{-i\omega/2}\left[\mathrm{e}^{i\alpha m} g\left(\varepsilon_m\left(\omega-\pi\left(m+\frac{1}{2}\right)\right)\right) + \mathrm{e}^{-i\alpha m} g\left(\varepsilon_{m+1}\left(\omega+\pi\left(m+\frac{1}{2}\right)\right)\right)\right] \tag{3}$$

where $\varepsilon_m = (-1)^m$ and $\alpha_m = (\pi/2)(m + (1/2))$. The properties of g have to ensure that

$$\sum_{m=0}^{\infty}\left|\hat{\psi}^0_m(\omega)\right|^2 = 1 \tag{4}$$

Then, the translates $\left\{\psi^0_m(.-n)\right\}$ form an orthonormal basis of $L^2(R)$. Introducing the basis functions

$$\psi^j_{m,n}(x) = \psi^j_m\left(x-2^{-j}n\right) = 2^{j/2}\psi^0_m\left(2^j x-n\right) \tag{5}$$

The transform $WA : L^2(R) \to l^2(Z)$ maps a function u onto a sequence of wave atom coefficients

$$c_{j,m,n} = \int_{-\infty}^{\infty} u(x)\psi^j_{m,n}(x)\mathrm{d}x = \frac{1}{2\pi}\int_{-\infty}^{\infty} \mathrm{e}^{-i2^{-j}n\omega}\overline{\hat{\psi}^j_m(\omega)}\hat{u}(\omega)\mathrm{d}\omega \tag{6}$$

In the 2-D case, Let $\mu = (j, m, n)$, where $m = (m_1, m_2)$ and $n = (n_1, n_2)$. We consider

$$\varphi^+_\mu(x_1, x_2) := \psi^j_{m_1,n_1}(x_1)\psi^j_{m_2,n_2}(x_2) \tag{7}$$

and the Hilbert transformed wavelet packets

$$\varphi^-_\mu(x_1, x_2) := H\psi^j_{m_1,n_1}(x_1)H\psi^j_{m_2,n_2}(x_2) \tag{8}$$

where for a decomposition $\hat{\psi}_{m,n}(\omega) = \hat{\psi}^j_{m,n,+}(\omega) + i\hat{\psi}^j_{m,n,-}(\omega)$ with $\hat{\psi}^j_{m,n,-}(\omega) = \overline{\hat{\psi}^j_{m,n,+}(\omega)}$ and the Hilbert transform is defined by

$$H\hat{\psi}^j_{m,n}(\omega) = -i\hat{\psi}^j_{m,n,+}(\omega) + i\hat{\psi}^j_{m,n,-}(\omega) \tag{9}$$

(Note that the above decomposition of $\hat{\psi}_{m,n}$ is possible since $\psi_{m,n}$ is real-valued). A recombination

$$\varphi^{(1)}_\mu = \frac{\varphi^+_\mu + \varphi^-_\mu}{2}, \quad \varphi^{(2)}_\mu = \frac{\varphi^-_\mu + \varphi^-_\mu}{2} \tag{10}$$

provides basis functions with two bumps in the frequency plane being symmetric with respect to the origin. Together, $\varphi^{(1)}_\mu$ and $\varphi^{(2)}_\mu$ form a wave atom frame, and the wave atom coefficients $c^{(1)}_\mu$, $c^{(2)}_\mu$ are the scalar products of u with $\varphi^{(1)}_\mu$ and $\varphi^{(2)}_\mu$.

Wave atoms have parabolic scaling in the sense that the period of the oscillations of each wave atom (wavelength) is linked to the square of the essential support (diameter). Also they are simultaneous directional and multiscale, that is, the wave atom is medium directional and scaling compared to the

poor directional and good scaling wavelet, good directional and poor scaling Gabor, good directional and good scaling Ridgelets and medium directional and good scaling Curvelet. The medium directionality and scaling is better [13] for texture classification. Due to these properties, the wave atom is considered for texture classification in this paper.

In [13], a discretization of this transform is described for the 1-D case, as well as an extension to two dimensions. The algorithm is based on the fast Fourier transform and a wrapping trick. The implementation software was downloaded from the web address http://www.waveatom.org/software.html.

2.2 Singular value decomposition

SVD is a very powerful tool, mainly used for dimensionality reduction. Since the number of transformed coefficients is large, computation cost is high. If SVD is applied on transformed coefficients, the number of resulting singular values is less than the number of transformed coefficients. We have found that the distribution of singular values of transformed coefficients varies vastly from texture to texture. This implies that distribution of the singular values possesses good discrimination characteristics.

Let A be the transformation coefficient matrix. If SVD is applied on A of size $P \times Q$, such that

$$A = U \Sigma V^T \tag{11}$$

Here, U is a $P \times Q$ orthogonal matrix whose columns are the eigenvectors of AA^T, V is a $Q \times Q$ orthogonal matrix whose columns are the eigenvectors of $A^T A$, and Σ is a $Q \times Q$ diagonal matrix with non-negative diagonal elements in decreasing order of magnitudes whose entries (the "singular values") are the square roots of the corresponding eigenvalues of AA^T.

2.3 Support vector machines

SVM is used for classification because of its powerful pattern classification capability [14]. An important advantage of the SVMs is that it is based on the principle of structural risk minimization. Besides, unlike other pattern recognition methods, SVMs do not depend explicitly on the dimensionality of the problem.

SVM finds the hyperplane that causes the largest separation between the decision function values for the borderline of the two classes. Mathematically, this hyperplane can be found by minimizing the cost function:

$$J(w) = w^T w = \|w\|^2 \tag{12}$$

Kernel representation offers an alternative solution by projecting the data into a high dimensional feature space to increase the computational power of the linear learning machines. A kernel is a function k, such that for all $x, z \in X$

$$k(x, z) = \langle \varphi(x), \varphi(z) \rangle \tag{13}$$

where φ is a mapping from X to (an inner product) feature space F. In this study, RBF kernel is used for classification. The main advantage of RBF kernel is their localized and finite responses.

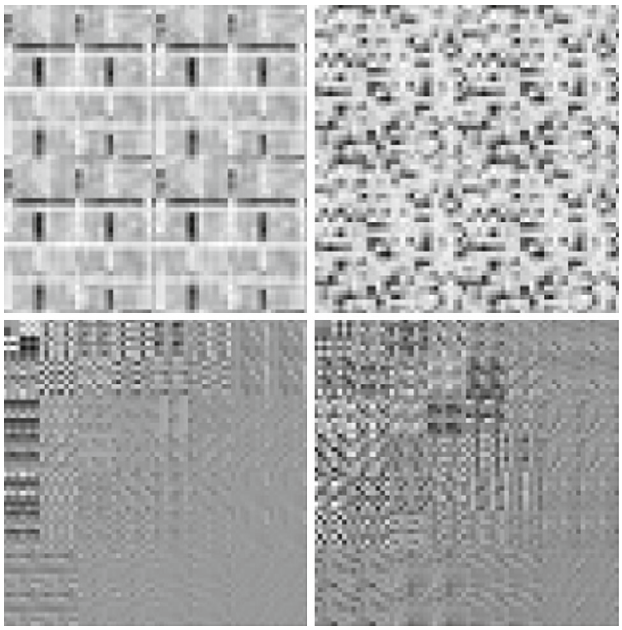

Fig. 1 First row shows two different textures from Brodatz data set and second row shows corresponding wave atom transform coefficients

3 Results and discussions

The performance of the wave atom in texture classification is analyzed on Brodatz database texture images, ADNI database for Alzheimer's disease and liver tumor classification on CT images.

3.1 Brodatz database texture images

Here Brodatz texture database [15] has been used as it is widely used for evaluating texture classification algorithms. Brodatz database consists of both homogeneous and non-homogeneous textures. The entire collection of 111 textures in Brodatz texture database is considered for training and testing phases. Each 512×512 images are divided into sixty-four, 64×64 non-overlapping sub-images. For training phase, one sub-image is randomly taken from each texture samples and for testing phase another sub-image is randomly taken from each texture samples. So a total of 111 texture samples are available for training and another 111 for testing.

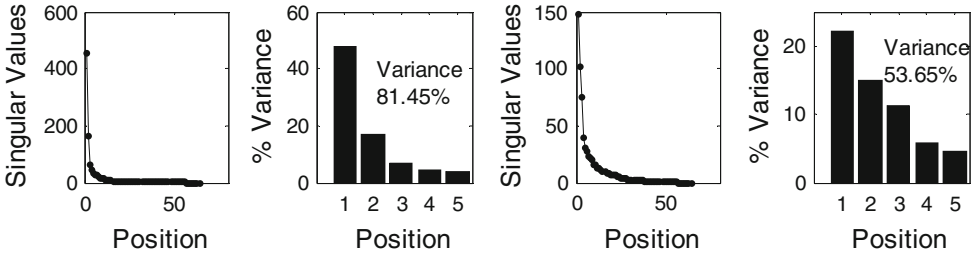

Fig. 2 SVD distribution and variance of first five SVD of D1 and D3 textures

The wave atom–transformed coefficients are determined for all samples, and SVD is applied on all transformed coefficients. Figure 1 shows two texture samples from Brodatz texture database and its wave atom–transformed coefficients. The SVD is applied on the wave atom transform coefficients to reduce the dimension. The distribution of SVD and the variance of first five SVD of D1 and D3 textures are given in Fig. 2. This shows that the variance of first five SVD is between 50 and 90 % for all textures. So from the SVD matrix, first five values are considered as the texture features for classification. In the training phase, SVD values for all sub-images are stored in the database. In the testing phase, the feature vector derived from the unknown image is compared with the feature vectors in the database using the distance vector formula, given in Eq. (14).

$$D(i) = \sum_{j=1}^{p} abs\left[f_j(x) - f_j(i)\right] \tag{14}$$

where P is the total number of features used, $i = 1$ to Q, (Q is the number of images in the database), $f_j(x)$ represents the jth feature of unknown texture image (x) and $f_j(i)$ represents the jth feature of texture belonging to ith texture. In classification, the unknown texture is assigned to nth texture if $D(n) < D(i)$ for all i; i not equal to n.

The percent correct classification is calculated using the Eq. (15).

$$G(\%) = \frac{C_{\text{corr}}}{M} \times 100\,\% \tag{15}$$

where, C_{corr} is the number of sub-images correctly classified and M is the total number of sub-images, derived from each texture image. In this method, we could be able to achieve the percent correct classification of 97.29 %, that is, out of 111 textures 108 were correctly classified and 3 were misclassified. Among 3 misclassified textures, 2 belongs to non-homogeneous and one belongs to homogeneous. Due to the close resemblance of textures, D23 and D27, D32 and D33, D3 and D22 were misclassified each other.

This method is also compared with the texture features taken through wavelet transform, gray level co-occurrence matrix (GLCM) and circular Gabor filter features. For wavelet-based texture features, 2 level decomposition and db4 wavelet basis function are used. From the available 35 texture features, 5 best features were selected using SVD. The percent correct classification for this method is 95.49 %. For GLCM-based classification, 5 best features were selected from the available 22 features using SVD. The percent correct classification for this method is 94.59 %. For circular Gabor filter-based classification, four circularly symmetric Gabor filter with center frequencies 2.00, 3.17, 5.04, and 8.00 are employed. The averaged response magnitude of each filtered image is utilized as one of the features. The feature vector has four dimensions. The percent correct classification for this method is 92.83 %.

3.2 Medical applications

The problem of Alzheimer's disease classification from MRI and liver tumor classification from CT images are chosen as specific applications of the texture classification is discussed herein to emphasize the effectiveness of our proposed feature extraction method. Different diseases have distinctive visual appearance. Thus, a block of diseased part may be regarded as a distinct texture pattern. This observation motivates us to utilize the texture classification algorithm for the Alzheimer's disease and tumor identification.

3.2.1 ADNI database for Alzheimer's disease

A total of 100 data sets were examined in this study. All data sets were selected from the Alzheimer's disease Neuroimaging Initiative (ADNI) database (www.loni.ucla.edu/ADNI). The MRI scans were acquired from multiple sites using either a GE or Siemens or Philips 3T system. High-resolution T1- weighted volumetric MP-RAGE scans were collected for each subject, and the MINC format images were downloaded from the public ADNI site (http://www.loni.ucla.edu/ADNI/Data/index.shtml). Parameter values vary depending on scanning site and can be found at http://www.loni.ucla.edu/ADNI/Research/Cores/. Out of 100 data sets, 40 belongs to AD brain T1-weighted MRI and 60 belongs to Normal brain T1-weighted MRI. From all the data sets, hippocampus is segmented from the coronal slice using the method adapted in [16]. The segmented hippocampus region is padded with zeros to make the size of the region into 32×32 in order to apply wave atom transform. Then, wave atom transform is applied to get the transformed image. The Fig. 3 shows the region of interest on AD MRI and normal MRI

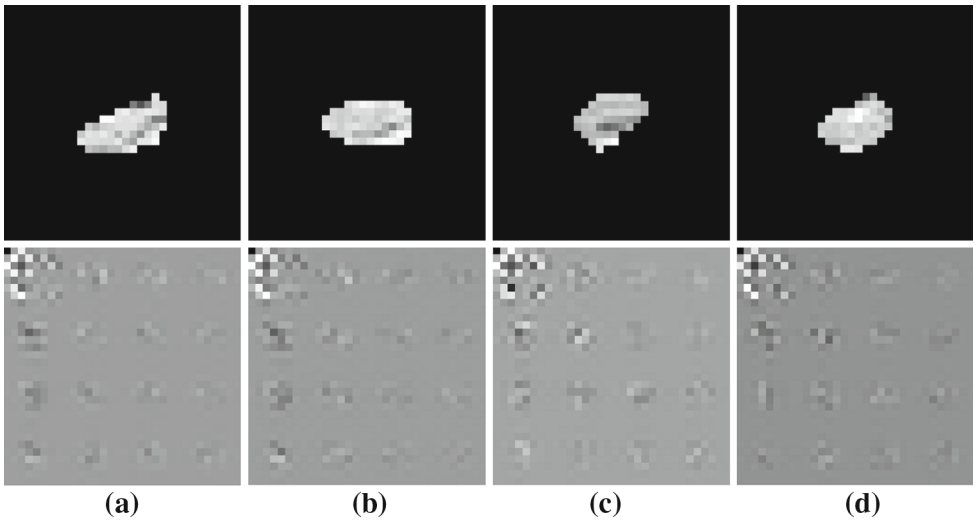

Fig. 3 First row MRI hippocampus images and second row corresponding wave atom transform coefficients (**a**, **b** for AD **c**, **d** for normal)

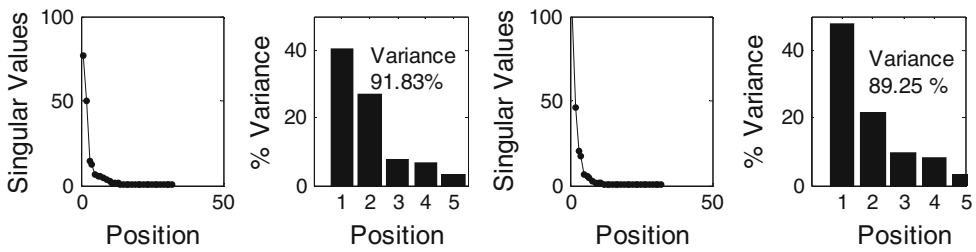

Fig. 4 SVD distribution and variance of first five SVD of normal and AD hippocampus textures

Table 1 Events that assign TP, FN, TN and FP

	Classified as AD	Classified as normal
Actually AD	TP	FN
Actually normal	FP	TN

and its transformed images. The transformed image pattern itself shows the discrimination. SVD is applied on the transformed coefficients. The SVD distribution and the variance of first five SVD is given in Fig. 4. Since the variance of first five SVD is close to 90 %, first five values are selected for classification.

To train and test the SVM, out of 40 AD features, 20 AD features were randomly assigned for training and remaining 20 AD features were assigned for testing and out of 60 Normal features, 30 Normal features were assigned for training and remaining 30 Normal features were assigned for testing.

To validate and quantify the effectiveness of the proposed texture feature extraction, and classification algorithm, four traditional performance metrics, namely Sensitivity, Accuracy, Specificity, and Precision, are measured [17]. Table 1 defines events that assign true positive (TP), false negative (FN), true negative (TN), and false positive (FP) used in the performance metrics equations defined as follows:

$$\text{Precision} = \frac{\text{TP}}{\text{TP} + \text{FP}} \quad \text{and}$$

$$\text{Sensitivity} = \frac{\text{TP}}{\text{TP} + \text{FN}} \tag{16}$$

$$\text{Specificity} = \frac{\text{TN}}{\text{FP} + \text{TN}} \quad \text{and}$$

$$\text{Accuracy} = \frac{\text{TP} + \text{TN}}{\text{TP} + \text{TN} + \text{FP} + \text{FN}} \tag{17}$$

The validation parameters Precision, Sensitivity, Specificity, and Accuracy for wave atom features are 94.7, 90, 96.7, and 94 % respectively. Among the two misclassified data sets belongs to AD, one is male and another is female and both are above 85 years old. One normal female aged 85 was misclassified as AD. This shows the wave atom feature extraction approach has the highest classification rate with good accuracy and precision.

This method is also compared with the texture features taken through wavelet transform, GLCM and circular Gabor filter features. The validation parameters Precision, Sensitivity, Specificity, and Accuracy for wavelet texture features are 85.7, 90, 90, and 90 % respectively. The 2 misclassified data sets belonging to AD are from a male and a female patient above 80 years old. The 3 misclassified data sets belong to Normal are from two male and a female patients who are above 85 years old. The performance of the proposed method is better compared to the previous cases. The validation parameters Precision, Sensitivity, Specificity, and Accuracy for GLCM are 85, 85, 90, and 88 % respectively. Here, the 3 misclassified data sets belonging to AD are from

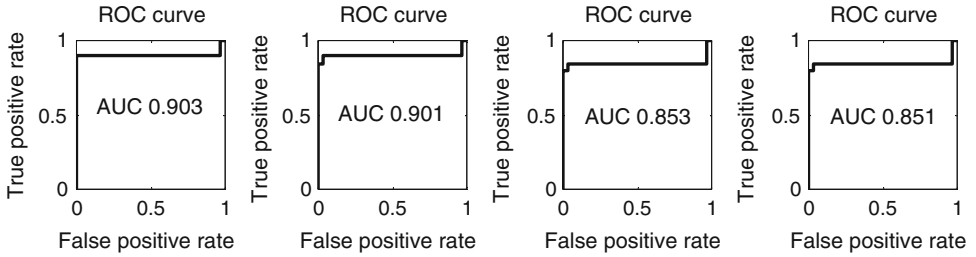

Fig. 5 ROC curve for the classifier in wave atom, wavelet transformed coefficient GLCM and Gabor filter texture features of MRI hippocampus

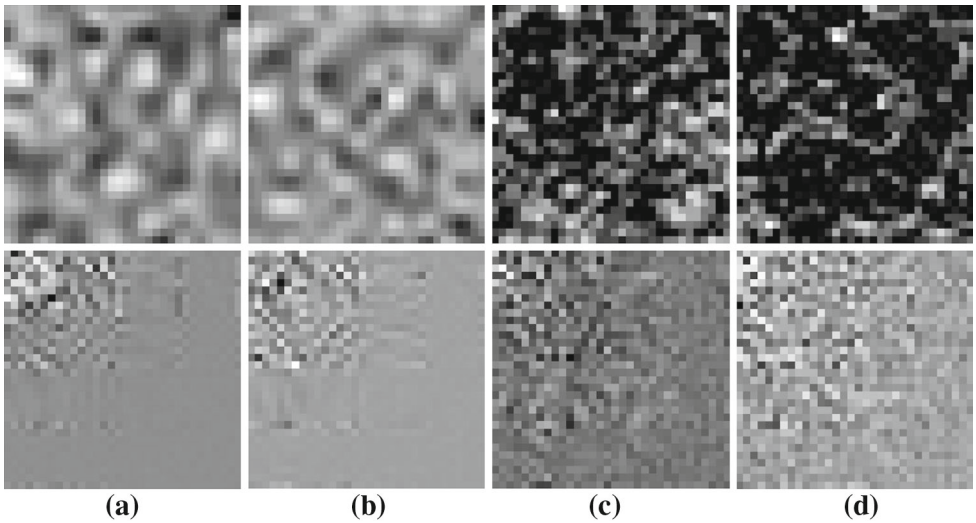

Fig. 6 First row is the sample CT images and second row is the corresponding wave atom transform coefficients (**a**, **b** for hemangioma **c**, **d** for hepatoma)

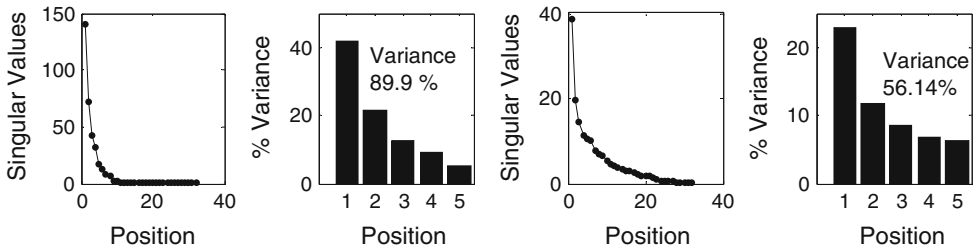

Fig. 7 SVD distribution and variance of first five SVD of hemangioma and hepatoma textures

patients above 85 years old, one belongs to male and other two belong to female patients. The 3 misclassified data sets belong to Normal are above 85 years old and one belongs to female and other two belong to male patients. The validation parameters Precision, Sensitivity, Specificity, and Accuracy for Gabor filter features are 81, 85, 86.7, and 86 % respectively. Here, the 3 misclassified data sets belonging to AD are from patients above 85 years old, one belongs to male and other two belongs to female patients. The 4 misclassified data sets belong to Normal are above 85 years old and one belongs to female and other three belong to male patients. The performances for the four methods are illustrated with ROC curve in Fig. 5.

3.2.2 Liver tumor classification on CT images

A total of 90 abdominal CT images considered in this work are collected from Regional Cancer Centre, Chennai on GE CT Scanner. Of which, 50 belong to benign (hemangioma) and other 40 belong to malignant (hepatoma) cases. All the used samples are of size 512 × 512 and slice thickness of 5 mm. A region of interest of 32 × 32 sizes within the segmented tumor region is cropped to apply wave atom transform-based feature extraction. Figure 6 shows the wave atom–transformed sub-band coefficients of the tumor region. As in Sect. 3.2.1, the SVD is applied to the sub-band coefficients. The SVD distribution and the variance of first five SVD are given in Fig. 7. Since the variance of first five SVD is between 50 and 90 %, the first five values are selected for classification using the same SVM classifier. Of the total 90 test data, 45 images are used for training the classifier and the other 45 are used for testing. The training set and testing sets contain 25 hemangioma and 20 hepatoma images, respectively. The classification results are evaluated using the performance measures used in Sect. 3.2.

The validation performance measures of the proposed method are compared with the performance measures

Table 2 Performance measures comparison of the four methods

	Accuracy (%)	Specificity (%)	Sensitivity (%)	Precision (%)
Wave atom	93.3	96	90	94.7
Wavelet transform	88.9	92	85	89.5
GLCM	84.4	84	85	81
Gabor filter	80	80	80	76.2

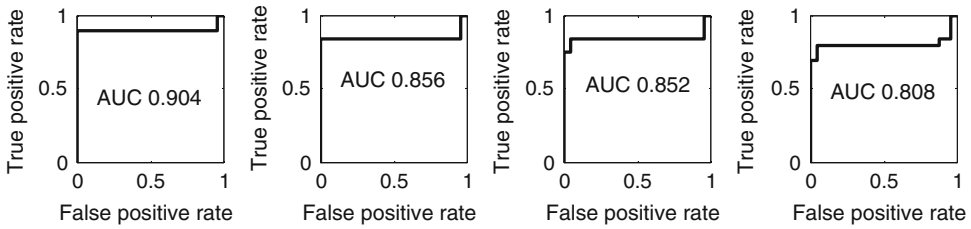

Fig. 8 ROC curve for the classifier in wave atom, wavelet transformed coefficient, GLCM and Gabor filter texture features of liver CT images

determined with the texture features calculated using wavelet transform, GLCM and circular Gabor filter features. The comparative performance measures are given in Table 2.

The performance measures comparison shows that the classification accuracy has considerably increased by the proposed method than the wavelet, GLCM and Gabor filter methods. The accuracy has increased by 4.4 % than wavelet, 8.9 % than GLCM, and 13.3 % than Gabor filter features. Among the 25 hemangioma features used for testing, 24 are classified correctly as hemangioma while 1 of them is misclassified as hepatoma. Of the 20 hepatoma cases, 18 are classified as hepatoma while the rest is classified as hemangioma using wave atom-based feature extraction. The misclassification rate using wave atom approach is much smaller than wavelet, GLCM, and Gabor filter feature approaches. The amount of misclassification using wavelet transform is higher than wave atom but lesser than GLCM-based feature extraction method. There are considerable improvements in other measures also. This is mainly due to the wave atom transform analysis-based texture features of tumor that has the ability to adapt to arbitrary local directions of pattern, and to sparsely represent anisotropic patterns. The ROC curves for the 4 methods of liver tumor diagnosis are shown in Fig. 8. The area under the curve (AUC) for the proposed method is greater than other techniques.

4 Conclusion

A useful texture feature extraction algorithm has been presented in this paper. The texture features are extracted using the wave atom transform and is significant for characterizing a texture. The effectiveness of the proposed features has been demonstrated in the texture classification experiments. It is proved that the wave atom transform is not only useful for the classification of synthetic features but also has the ability to discriminate the Alzheimer's disease using MRI brain images and liver tumor identification using CT images. Wave atom transform-based texture classification performance measures are high in comparison with wavelet transform, GLCM, and Gabor filter-based texture feature classification. Hence, wave atom transform-based feature extraction can be used for detecting and diagnosing several diseases.

Acknowledgments The authors would like to thank the Washington University Alzheimer's Disease Research Centre directed by John C. Moris, for providing clinical and imaging data, Dr. T. Muthu Retnam of Muthu Neuro Centre for giving the details of hippocampus anatomy and Dr. B. Jeyananda Sunil of Regional Cancer Centre, Chennai for providing liver CT images.

References

1. Ohanian, P.P., Dubes, R.C.: Performance evaluation for four classes of textural features. Pattern Recognit. **25**, 819–833 (1992)
2. Cohen, F.S., Fan, Z., Attali, S.: Automated inspection of textile fabrics using textural models. In: IEEE Trans. Pattern Anal. Mach. Intell. **13**, 803–808 (1991)
3. Hong, T.H., Dyer, C.R., Rosenfeld, A.: Texture primitive extraction using an edge-based approach. In: IEEE Trans. Syst. Man Cybern. **10**, 659–675 (1980)
4. Azencott, R., Jia-Ping, W., Younes, L.: Texture classification using windowed Fourier filters. In: IEEE Trans. Pattern Anal. Mach. Intell. **19**, 148–153 (1997)
5. Chang, T., Kuo, J.: Texture analysis and classification with tree-structured wavelet transform. In: IEEE Trans. Image Process. **2**, 429–441 (1993)
6. Unser, M., Eden, M.: Multiresolution feature extraction and selection for texture segmentation. In: IEEE Trans. Pattern Anal. Mach. Intell. **11**, 717–728 (1989)
7. Unser, M.: Texture classification and segmentation using wavelet frames. In: IEEE Trans. Image Process. **4**, 1549–1560 (1995)
8. Choi, H., Baraniuk, R.: Multiscale image segmentation using wavelet-domain hidden Markov models. In: IEEE Trans. Image Process. **10**, 1309–1321 (1998)
9. Do, M.M., Vetterli, M.: Wavelet-based texture retrieval using generalized Gaussian density and Kullback–Leibler distance. In: IEEE Trans. Image Process. **11**, 146–158 (2002)

10. Wouwer, G.V., Scheunders, P., Dyck, D.V.: Statistical texture characterization from discrete wavelet representations. In: IEEE Trans. Image Process. **8**, 592–598 (1999)
11. Chen, L., Man, H.: Hybrid IMM/SVM approach for wavelet-domain probabilistic model based texture classification. IEE Proc. Vis. Image Signal Process. **152**, 724–730 (2005)
12. Selvan, S., Ramakrishnan, S.: SVD-based modeling for image texture classification using wavelet transformation. In: IEEE Trans. Image Process. **16**, 2688–2696 (2007)
13. Demanet, L., Ying, L.: Wave atoms and sparsity of oscillatory patterns. Appl Comput. Harmon Anal. **23**, 368–387 (2007)
14. Brodatz, P.: Textures: A Photographic Album for Artists and Designers. Dover, New York, NY (1966)
15. Cristianini, N., Taylor, J.S.: An Introduction to Support Vector Machines and other Kernel-Based Learning. Cambridge University Press, (2000)
16. Rajeesh, J., Moni, R.S., Palanikumar, S., Gopalakrishnan, T.: A versatile algorithm for the automatic segmentation of hippocampus based on level set. Int. J. Biomed. Eng. Technol. **7**(3), 213–224 (2011)
17. Lao, Z., Shen, D., Xue, Z.: Morphological classification of brains via high-dimensional shape transformations and machine learning methods. Neuroimage **21**, 46–57 (2004)